International Journal of Engineering and Science Invention (IJESI)
ISSN (Online): 2319-6734, ISSN (Print): 2319-6726
www.ijesi.org ||Volume 14 Issue 6 June 2025 || PP 82-95

The Convective Heat Transfer Characteristics of the Array Fins Moving in the Direction of Movement

Jun He[1,2], Xin Lu[1,2], Liang-Bi Wang[1,2]
[1](School of Electrical and Mechanical Engineering, Lanzhou Jiaotong University, China)
[2](Key Laboratory of Thermal Engineering of Railway Vehicles, Ministry of Education, Lanzhou Jiaotong University, China)

ABSTRACT : *Convective heat transfer caused by the movement of array fins in the direction of movement is more common in the heat transfer phenomenon caused by the installation of array fins on the outer surface of moving objects. The paper numerically simulated the convective heat transfer characteristics of the array fins moving in the direction of movement by using the layering dynamic grid technology, and obtained the variation laws of the air flow rate in the fin channel, the surface convective heat transfer coefficient, thermal resistance, fin efficiency and heat transfer coefficient under different moving speeds, as well as the influence of fin structure parameters on the comprehensive performance of the fin. The results show that as the moving speed of the fins increases, the surface convective heat transfer coefficient of the fin channel increases, the convective heat transfer capacity enhances, the thermal resistance decreases, and the moving speed has the greatest influence on the convective thermal resistance. Unlike the common channel, the flow rates at the inlet and outlet sections of the fin channel are not equal. Therefore, the logarithmic mean temperature difference cannot be used to calculate the overall heat transfer coefficient. For this problem, the paper uses the integral method to calculate the average temperature difference of the heat transfer process, and the heat transfer coefficient increases with the increase of the moving speed. Both the comprehensive performance of the fins and the fin efficiency decrease with the increase of the moving speed, indicating that the comprehensive performance of the fins decreases with the increase of the moving speed. The order of the influence of fin structure on the comprehensive performance of fins is as follows: fin thickness,fin length,fin height,and fin spacing.*

KEYWORDS -*Convection Heat Transfer; Dynamic Mesh ; Moving Fins; Numerical Simulation*

Date of Submission: 15-06-2025 Date of Acceptance: 30-06-2025

I.INTRODUCTION

With the rapid development of power semiconductor technology [1] and the continuous increase in the speed of high-speed trains, the demand for efficient, compact and low-energy consumption cooling solutions is becoming increasingly urgent. Train-induced airflow cooling [2] has shown significant advantages as a new type of cooling method. This technology utilizes the powerful outward swept airflow generated when the train is running at high speed to replace the traditional forced air cooling or liquid cooling systems. It features a simple structure, small volume and weight, and effective reduction of auxiliary energy consumption and noise, providing a highly promising solution for the heat dissipation of high-power-density equipment.

At present, domestic and foreign scholars have begun to pay attention to and explore the potential and application of this emerging cooling technology. Pang et al.[3] put forward forward-looking suggestions on the technical path and product development of the application of train-induced airflow cooling in train traction equipment from a macro perspective. Jin[4] successfully designed and implemented the first domestic Train-induced airflow-cooled traction transformer applied to EMUs, verifying the feasibility of this technology. In terms of optimizing the airflow organization,Ma et al.[5] effectively enhanced the heat dissipation capacity of the Train-induced air by adding deflector plates to adjust the flow distribution under the vehicle. Luo et al.[6] obtained the empirical relationship between the wind speed around the traction converter of intercity EMUs and the running speed of the train through research, providing an important reference for the system design. Huang et al.[7] focused on the influence of vehicle layout on heat dissipation performance, providing guiding suggestions for the overall design of the Train-induced airflow cooling system. Meanwhile, research on the heat transfer characteristics and enhanced heat transfer of traditional fixed finned heat sinks has been quite in-depth and extensive[8-13], covering the influence laws of finned resistance characteristics, heat transfer characteristics, and key structural parameters (such as shape, spacing, height, length, etc.) on heat dissipation performance, and deeply exploring the roles of factors such as the flow rate and physical properties of the cooling medium.

Systematic basic research on the new cooling method of train-induced airflow cooling, especially the research on the heat transfer characteristics of array fins whose core heat dissipation components are directly exposed to high-speed running air, is still relatively scarce, and the available experimental data for reference is extremely limited. The existing research results on enhanced heat transfer by fins are almost all based on wind tunnel simulations or experiments, that is, the active impact of fluids on stationary objects. However, in the practical application scenario of train-induced airflow cooling, the fins are located on the surface of the high-speed moving train and actively collide with the relatively stationary air. This paper focuses on the core scientific issue of the forced convective heat transfer characteristics of the array fins on the outer surface of a moving object under high-speed motion conditions. It adopts layering dynamic grid technology to restore the real motion of the moving object, aiming to reveal the flow and heat transfer laws of the fin array in this special scenario and provides a reference for the design and application of heat sinks for this new type of cooling method.

II.PHYSICAL MODEL

The air-cooling method with array fins on the outer surface of a moving object involves placing a semiconductor component as the heat source on a heat sink. The heat sink is composed of multiple heat dissipation fins arranged on the surface of the moving object. When the object moves, the outward swept airflow exchanges convective heat with the heat dissipation fins, as shown in Fig. 1.

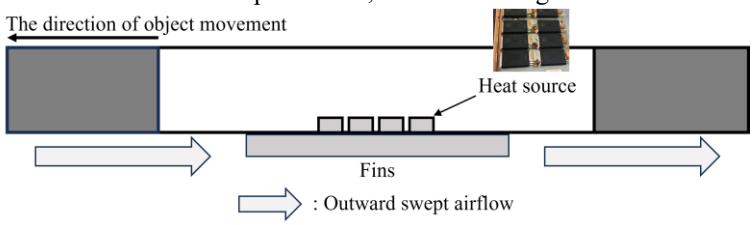

Figure.1 Schematic diagram of the cooling method

Fig. 2 is a three-dimensional schematic diagram of the heat sink, in which the length L of the heat sink is 500 mm, the width W is 175 mm, and the height H is 110 mm. The partial schematic diagram of the heat sink is shown in the red dashed box. Among them, the fin spacing s is 15 mm, the fin thickness t is 4 mm, the fin height h is 100 mm, and the base plate thickness b is 10 mm.

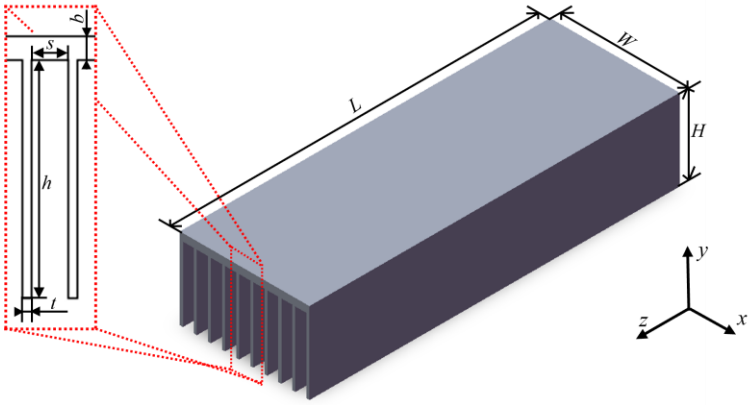

Figure.2 Three-dimensional model of the heat sink

III. NUMERICAL MODEL

3.1 Control Equation

The cooling medium in the paper is air. When the maximum moving speed of the fins is 100 m/s, the Mach number is less than 0.3. Therefore, in the calculation, air is considered an incompressible fluid, and the physical property parameters are constant. Radiative heat transfer is ignored, and only convective heat transfer and heat conduction are considered. The physical property parameters of air (15℃) and the heat sink material aluminum are shown in Table 1.

Table 1 Physical parameters of air and aluminum

Material	Densityρ(Kg/m^3)	Thermal conductivity coefficientλ(W/(m·K))	Specific heat capacityC_p(J/(kg·K))
Air	1.225	0.0242	1006
Aluminum	2719	202	8710

In the paper, the moving speed of the array fins reached the fastest 100 m/s, and the corresponding Reynolds number exceeded 10^4. Therefore, the Standard k-ε model and the wall function method were selected for numerical simulation. The control equation of the fluid region is as follows:

Continuity equation:

$$\frac{\partial u_i}{\partial x_i} = 0 \tag{1}$$

where,u_i is the velocity component.

Momentum equation:

$$\frac{\partial}{\partial x_j}\left(u_i u_j\right) = \frac{\partial}{\partial x_j}\left((\mu + \mu_t)\frac{\partial u_i}{\partial x_j}\right) - \frac{\partial p}{\partial x_i} \tag{2}$$

$$\mu_t = \rho C_\mu \frac{k^2}{\varepsilon} \tag{3}$$

where,μ is the dynamic viscosity, μ_t is the turbulence viscosity coefficient,p stands for pressure, C_μ=0.09.

For the Standard k-ε model, k and $\varepsilon$are given below:

$$\frac{\partial(\rho k u_j)}{\partial x_j} = \frac{\partial}{\partial x_j}\left[\left(\mu + \frac{\mu_t}{\sigma_k}\right)\frac{\partial k}{\partial x_j}\right] + G_k - \rho\varepsilon \tag{4}$$

$$\frac{\partial(\rho\varepsilon u_j)}{\partial x_j} = \frac{\partial}{\partial x_j}\left[\left(\mu + \frac{\mu_t}{\sigma_\varepsilon}\right)\frac{\partial \varepsilon}{\partial x_j}\right] + C_{1\varepsilon}\frac{\varepsilon}{k}G_k - C_{2\varepsilon}\rho\frac{\varepsilon^2}{k} \tag{5}$$

In the above expressions, G_k represents the turbulent kinetic energy caused by the velocity gradient,σ_k=1.0, σ_ε=1.3, $C_{1\varepsilon}$=1.44, $C_{2\varepsilon}$=1.92.

Energy equation of fluid region:

$$\frac{\partial}{\partial x_j}(\rho u_j T) = \frac{\partial}{\partial x_j}\left(\rho(a + \frac{\mu_t}{\rho Pr_t})\frac{\partial T}{\partial x_j}\right) \tag{6}$$

where, a is the thermal diffusion coefficient.

The heat conduction equation in the solid region:

$$\frac{\partial T}{\partial t} = a\left(\frac{\partial^2 T}{\partial x_j^{\,2}}\right) \tag{7}$$

3.2 Calculation region and boundary conditions

As shown in Fig. 3, the blue area represents the air zone between the surface of the moving object and the ground, where the heat sink is located. The gray area represents the free air zone in front of the moving object. The width W_{tot} of the air domain between the surface of the moving object and the ground is 675 mm, the height H_{tot} is 200 mm, and the length L_{air} is 1750 mm. Due to the excessive length of the gray area, it is not fully displayed in the Fig.3, and its length L_{out} is 100 m. Boundary conditions: The upper and lower surfaces of the blue area are adiabatic walls. The surrounding surfaces of the blue area and the surrounding and upper surfaces of the gray area are pressure outlets, and the reflux temperature is 15℃. The given heat flux density of the red surface is 30000 W/m². The windward side, leeward side and the top surface of the fin are insulated and non-slip walls. The remaining fluid-solid contact surfaces are all coupled heat transfer walls without slip.

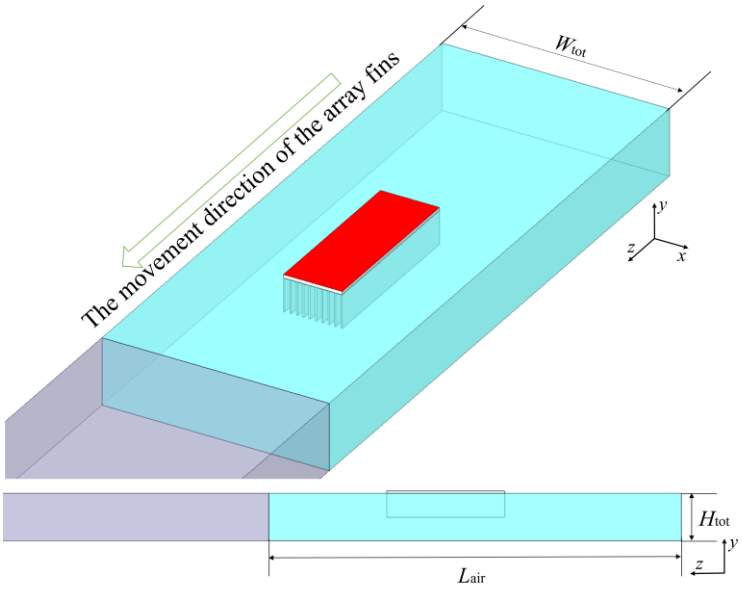

Figure.3 Schematic diagram of the computing domain

3.3 The expression parameters of the numerical results

As shown in Fig. 4, it is a schematic diagram of the fin channel. From Fig. 4, the fin channel is different from the ordinary channel. The ordinary channel only includes the inlet section and the outlet section, while the fin channel also has a section parallel to the flow direction. Air enters from the inlet section, part of it flows out from the outlet section, and the other part flows out from the section parallel to the flow direction.

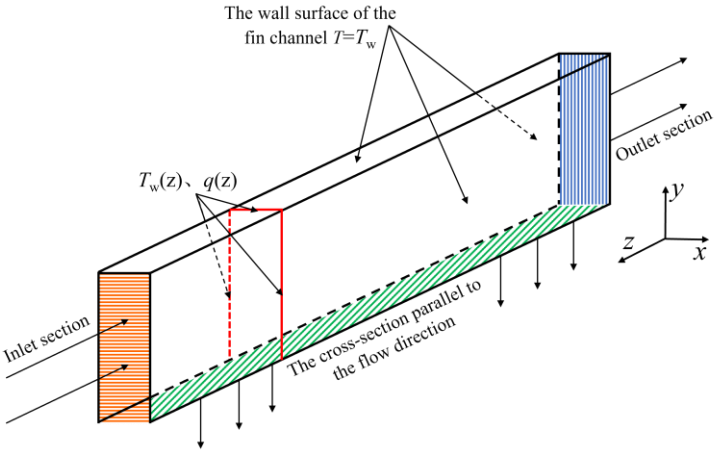

Figure.4 Schematic diagram of the fin channel

The parameter definitions and calculation formulas in the paper are as follows:

Reynolds number of the fin channel:

$$Re = \rho v_m D_h / \mu \tag{8}$$

Characteristic flow velocity of air in the fin channel:

$$v_m = \frac{1}{L}\int_0^L (v - v(z))dz \tag{9}$$

where, v represents the moving speed of the fins.

Average air flow velocity in the cross-section of the fin channel:

$$v(z) = \frac{1}{S}\iint_S v(x,y)dS \tag{10}$$

where, $v(x,y)$ represents the local air flow velocity on the cross-section of the rib channel.

Characteristic dimensions of the fin channel:

$$D_{\mathrm{h}} = \frac{4S}{P} = \frac{4hs}{2h+s} \tag{11}$$

Local heat flux density on the surface of the fin channel:

$$q_{\mathrm{local}} = -\lambda \left.\frac{\partial T}{\partial n}\right|_{\mathrm{w}} \tag{12}$$

The transverse average local convective heat transfer coefficient on the surface of the fin channel:

$$h_{\mathrm{s}}(z) = \frac{q(z)}{T_{\mathrm{w}}(z) - T_{\mathrm{f}}(z)} \tag{13}$$

The transverse average local heat flux density on the surface of the fin channel:

$$q(z) = \iint_{A(z)} q_{\mathrm{local}} dA dz \,/\, \iint_{A(z)} dA dz \tag{14}$$

The transverse average local temperature of the fin channel surface:

$$T_{\mathrm{w}}(z) = \iint_{A(z)} T_{\mathrm{w}}(x,y,z) dA dz \,/\, \iint_{A(z)} dA dz \tag{15}$$

where, $T_{\mathrm{w}}(x,y,z)$ represents the local wall surface temperature of the rib channel.

The average temperature of the fluid in the cross-section of the fin channel:

$$T_{\mathrm{f}}(z) = \frac{1}{S} \iint_{S} T_{\mathrm{f}}(x,y) dS \tag{16}$$

where, $T_{\mathrm{f}}(x,y)$ is the local air temperature on the cross-section of the channel.

Cross-sectional area of the fin channel:

$$S = hs \tag{17}$$

Heat dissipation on the surface of the fin channel:

$$Q = \iint_{A} q_{\mathrm{local}} dA \tag{18}$$

Average convective heat transfer coefficient on the surface of the fin channel:

$$h_{\mathrm{avg}} = Q \,/\, A(T_{\mathrm{w}} - T_{\mathrm{f}}) \tag{19}$$

The heat exchange area on the surface of the fin channel:

$$A = 2hL + sL \tag{20}$$

Average temperature of the fin surface:

$$T_{\mathrm{w}} = \frac{1}{A} \iint_{A} T_{\mathrm{w}}(x,y,z) dA \tag{21}$$

Average temperature of the fluid in the fin channel:

$$T_{\mathrm{f}} = \frac{1}{L} \int_{0}^{L} T_{\mathrm{f}}(z) dz \tag{22}$$

Average temperature of the fin base:

$$T_{\mathrm{h}} = \frac{1}{L} \int_{0}^{L} T_{\mathrm{h}}(z) dz \tag{23}$$

The fin efficiency η is a dimensional parameter that measures the ratio of the actual heat transfer capacity of the fin to the ideal heat transfer capacity[14]. In this paper, numerical simulation was used to respectively calculate the actual heat dissipation Q of the fin and the heat dissipation Q_{ideal} when the surface temperature of the fin is the temperature of the fin root. The calculation formulas are as follows:

$$\eta = Q \,/\, Q_{\mathrm{ideal}} \tag{24}$$

The total thermal resistance R in the paper is composed of the average thermal conduction resistance R_{cond} within the solid and the average convective thermal resistance R_{conv} at the fluid-solid contact surface. The fin channel thermal resistance model is shown in Fig. 5, and the formula is as follows:

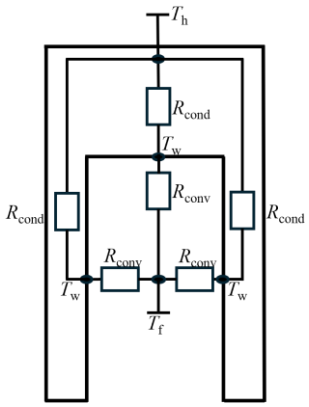

Figure.5Thermal resistance model

Total thermal resistance:

$$R = R_{cond} + R_{conv} \tag{25}$$

Average thermal conduction resistance:

$$R_{cond} = (T_h - T_w) / Q \tag{26}$$

Average convective thermal resistance:

$$R_{conv} = (T_w - T_f) / Q \tag{27}$$

The heat transfer coefficient K encompasses the entire heat transfer process. The heat transfer in the paper includes heat conduction inside the heat sink and convective heat transfer between the surface of the fins and the air. Since the air flow at the inlet and outlet of the fin channel is not conserved, the average temperature difference Δt_m cannot be calculated by the logarithmic mean temperature difference. Therefore, the average temperature difference in the heat transfer process of the fin channel is calculated by the integral method, as shown in Fig. 6.

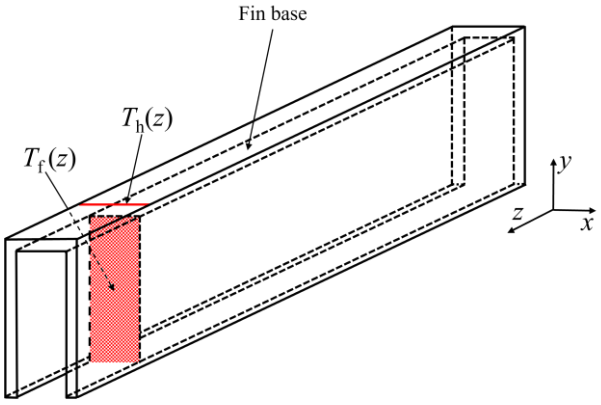

Figure.6 Schematic diagram of the integration method for the average temperature difference

Average temperature difference:

$$\Delta t_m = \frac{1}{L}\int_0^L \left(T_h(z) - T_f(z)\right)dz \tag{28}$$

Heat transfer coefficient:

$$K = Q / A\Delta t_m \tag{29}$$

The paper introduces the heat transfer factor and the resistance coefficient to evaluate the heat transfer and resistance characteristics of the fins. Meanwhile, the comprehensive performance coefficient E[15] of the fins and the relative comprehensive performance E_p under the condition of the same pump power are introduced to evaluate the comprehensive performance of the fins. The calculation formulasare as follows:

Average heat transfer factor on the surface of the fin:

$$j = h_{avg} Pr^{2/3} / \rho v C_p \tag{30}$$

The resistance coefficient of the fin:

$$f = 2F_d / \rho v^2 A_s \tag{31}$$

$$A_s = ht \tag{32}$$

where, F_d is the resistance during the movement of the fin, A_s is the reference area.

Comprehensive performance coefficient:

$$E = j / f^{1/3} \tag{33}$$

The comprehensive performance coefficient under the condition of equal pump power:

$$E_p = (j / j_{ref}) / (f / f_{ref})^{1/3} \tag{34}$$

3.4 Grid division and layering dynamic grid technology

The model in the paper has a regular shape and is highly suitable for dividing it into structured grids. The layering dynamic mesh technology[16] is to dynamically add or delete mesh layers in the adjacent areas of the motion boundary, and segment or merge the mesh layers according to the displacement threshold. The paper selects to merge the grids on the motion boundary based on the grid height, setting the merging factor α_c, with h_{min} as the minimum element height and h_0 as the original element height. When $h_{min}<\alpha_c h_0$, the grids will merge with the next layer of grids, as shown in Fig. 7.

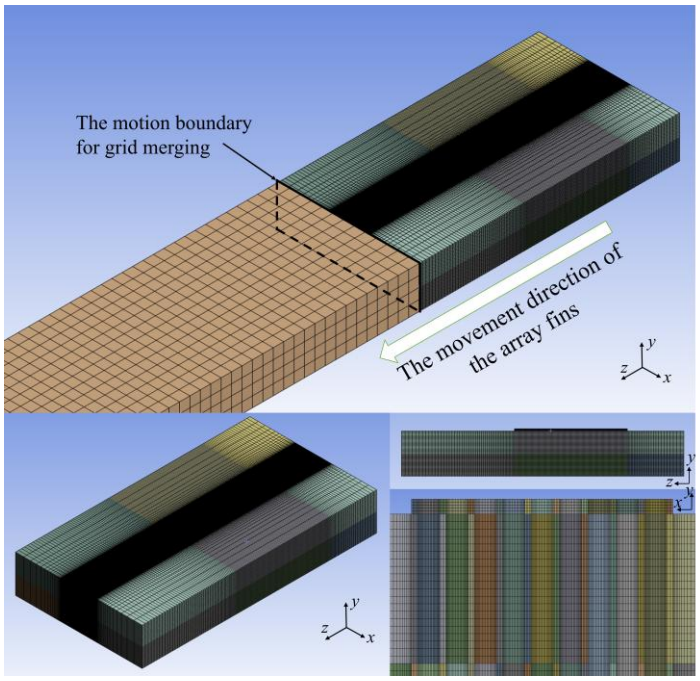

Figure.7 Schematic diagram of grid division and layering dynamic grid

2.5 Verification of Grid Independence and Numerical Results

The paper selects three grid schemes when the moving speed is 50 m/s. The height of the boundary layer grid remains unchanged, and the air domain grid outside the boundary layer is gradually encrypted. The grid independence verification is shown in Table 2. The number of grids has a relatively small influence on the calculation results, which meets the requirements of the independence verification. Considering the limited computing resources, a grid of 6.4 million was selected for numerical calculation.

Table 2 Grid independence verification

Plan	The number of grids	h_{avg}(W/(m^2·K))	Relative error (%)
1	6.4×10^6	154.61	—
2	8.2×10^6	154.86	0.162%
3	10.1×10^6	155.07	0.297%

Before conducting numerical simulation, the numerical results need to be verified. The correlations are as follows:

$$Nu_{D\text{-}B} = 0.023 Re^{0.8} Pr^{0.4} \tag{35}$$

$$Nu_G = \frac{(c/8)(Re-1000)Pr}{1+12.7\sqrt{c/8}(Pr^{2/3}-1)}\left(1+\left(\frac{D_h}{L}\right)^{2/3}\right) \tag{36}$$

$$c = (1.8 \lg Re - 1.5)^{-2} \tag{37}$$

As shown in Fig. 8, it is a comparison between the numerical simulation results and the results of the two correlations. The numerical results are basically consistent with the results of the correlation, among which the maximum relative error is 5.17%, and the error is within the acceptable range.

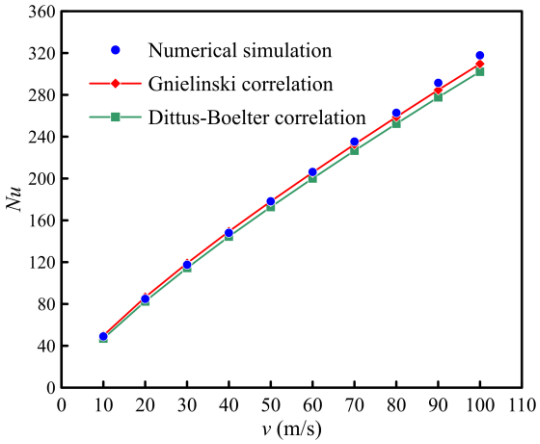

Figure.8 Verification of numerical results

IV.RESULTS AND ANALYSIS

4.1 Air flow at the inlet and outlet of the fin channel

During the movement of the object, air enters from the inlet section of the fin channel. Since the fin channel is connected to the surrounding air on three sides, the air will flow out from the outlet section of the fin channel and the section parallel to the flow direction. This results in unequal air flow rates at the inlet and outlet sections of the fin channel. The air flow rate at the inlet and outlet of the fin channel will change with the moving speed of the fin, and its variation trend is shown in Fig. 9.

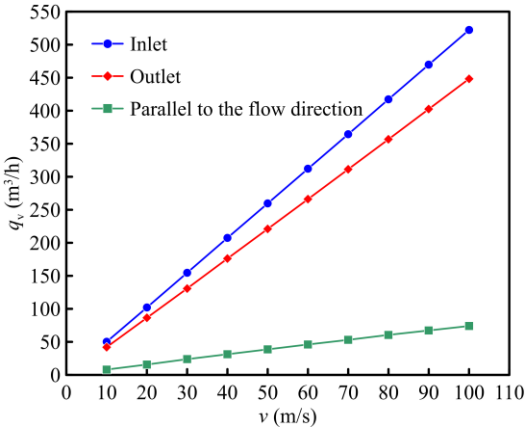

Figure.9 The variation of air flow rate in the cross-section of the fin channel under different moving speeds

The length of the fin channel also has an impact on the flow rate passing through the inlet and outlet sections of the fin channel. As shown in Fig. 10, it is the variation trend of the flow rate ratio passing through the outlet section to the inlet section of the fin channel with the length of the fin channel when the fin moving speed is 50 m/s, L_0=0.1 m. As the length of the fin channel increases, the ratio of the flow rates at the outlet and inlet sections of the fin channel gradually decreases. That is, the flow rate through the outlet section of the fin channel becomes smaller and smaller, while the flow rate through the section parallel to the flow direction becomes larger and larger.

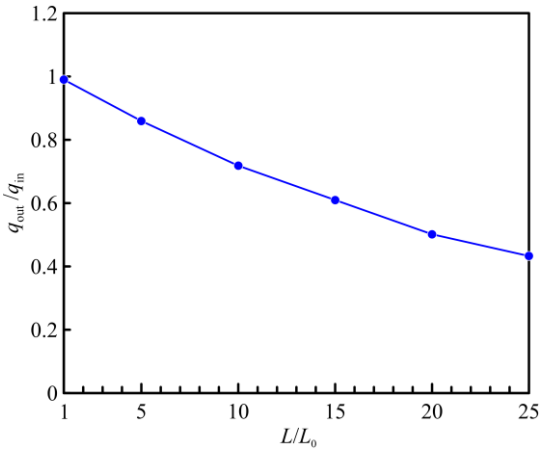

Figure.10 The variation trend of the ratio of the inlet and outlet flow rates of the fin channel with the length of the fin channel

4.2 Convective heat transfer coefficient of the fin surface

As shown in Fig. 11, with the continuous increase of the moving speed of the fins, the surface convective heat transfer coefficient of the fin channel becomes larger and larger, but the growth rate is gradually slowing down.

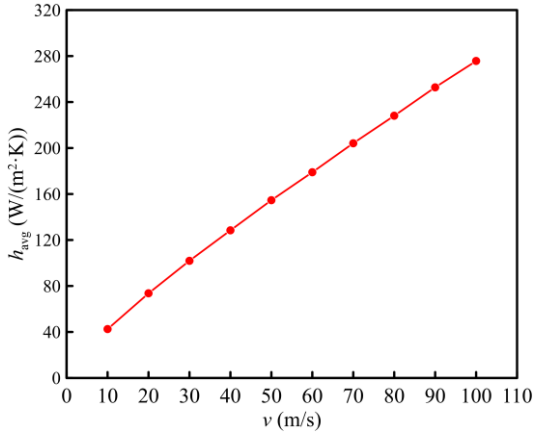

Figure.11 The average convective heat transfer coefficient of the fin channel surface under different moving speeds

Fig. 12 shows the variation of the transverse average local convective heat transfer coefficient in the fin channel. The transverse average local convective heat transfer coefficient in the fin channel gradually decreases along the length of the fin. The convective heat transfer coefficient at the inlet section of the ribbed channel is the largest, and that at the outlet section is the smallest.

4.3 Thermal resistance of heat transfer

As the moving speed of the object changes, the thermal resistance of the heat sink and the surface temperature of the heat sink will also change. As shown in Fig. 13, the variation laws of the thermal resistance of the heat sink, the temperature difference between the surface of the base plate and the surface of the fin channel, and the temperature difference between the surface of the fin channel and the air with the moving speed are presented. As the moving speed increases, the total thermal resistance, the thermal conduction resistance and the convective thermal resistance all show a downward trend. The proportion of the thermal conduction resistance in the total thermal resistance becomes larger and larger. The decreasing speed of thermal conduction resistance is slower than that of the convective thermal resistance. This is mainly because as the moving speed increases, The temperature difference between the surface of the fin channel and the air decreases at a faster rate than that between the surface of the substrate and the surface of the fin channel.

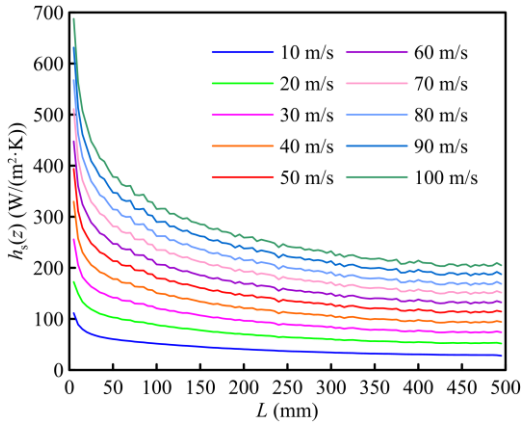

Figure.12 The variation of the transverse average local convective heat transfer coefficient of the fin channel

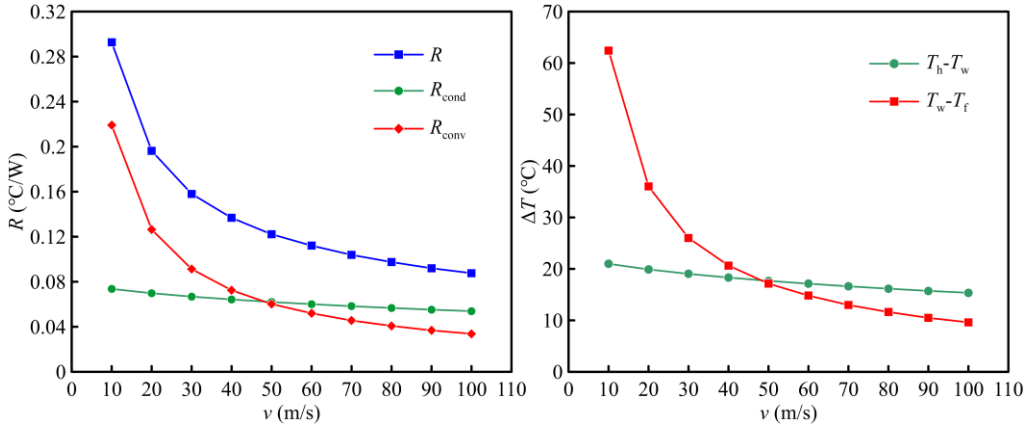

Figure.13 The variation law of the thermal resistance of the heat sink and the temperature difference on the heat sink surface with the moving speed

4.4Finefficiency

The fin efficiency is the ratio of the actual heat dissipation on the fin surface to the heat dissipation under the condition of equal wall temperature on the fin surface. As shown in Fig. 14, the fin efficiency η gradually decreases with the increase of the moving speed. The reason for the decline in fin efficiency is that as the moving speed increases, convective heat transfer intensifies, and heat is rapidly dissipated at the root of the fins, while the contribution of the distal end of the fins to heat dissipation is small.

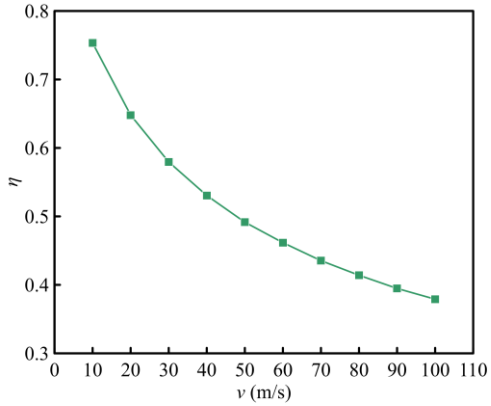

Figure.14 The variation law of fin efficiency with the moving speed

4.5 Heat transfer coefficient

The variation law of the heat transfer coefficient K of the average temperature difference in the heat transfer process calculated by the integration method with the moving speed of the fins is shown in Fig. 15. As the moving speed of the fins continuously increases, the heat transfer coefficient K also gradually increases. This indicates that the greater the moving speed, the more intense the entire heat transfer process, but the growth rate of the heat transfer coefficient is constantly decreasing.

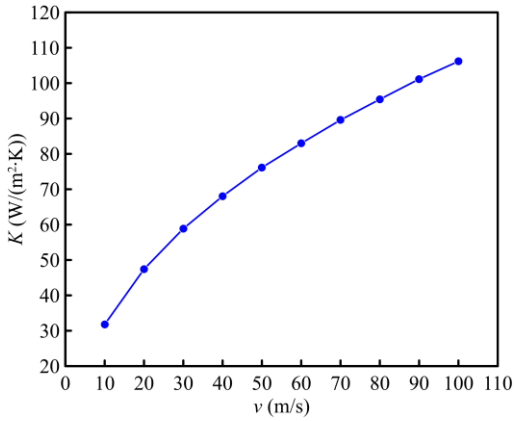

Figure.15 The variation law of the heat transfer coefficient with the moving speed

4.6 Evaluation of fin performance

The variation laws of the resistance factor *f* and the heat transfer factor *j* with the moving speed are shown in Fig. 16. Both the resistance factor *f* and the heat transfer factor *j* monotonically decrease with the increase of the moving speed, and the speed gradually decreases as it decreases.

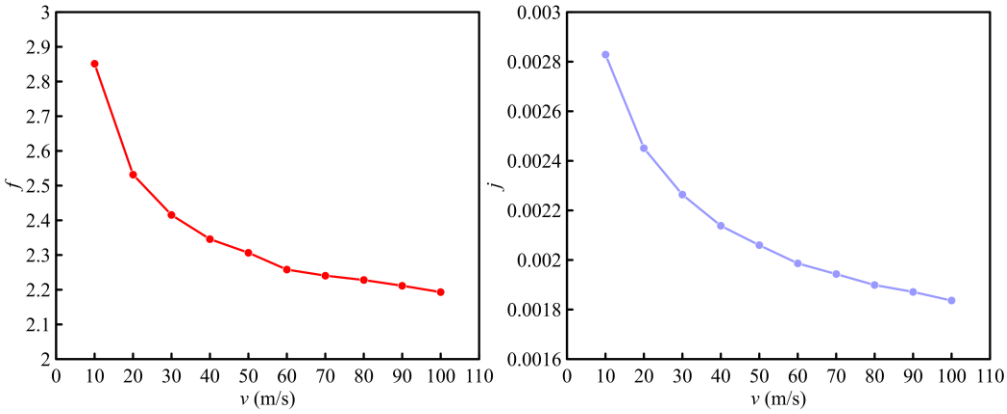

Figure.16 The variation laws of the resistance factor and the heat transfer factor with the moving speed of the fins

Taking the resistance coefficient and heat transfer factor when the fin moving speed is 10 m/s as reference values, the variation law of the comprehensive performance coefficient E_p with the fin moving speed under the condition of equal pump power is shown in Fig. 17. It can be seen from Fig. 17 that the comprehensive performance coefficient E_p monotonically decreases with the increase of the moving speed.

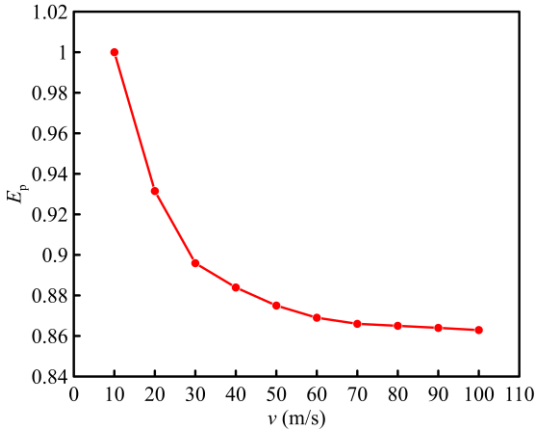

Figure.17 The variation law of the comprehensive performance *E*p with the moving speed

4.7 The influence of fin structure parameters on the performance of the heat sink

The thesis studies the influence of structural parameters on the comprehensive performance of the heat sink by using the Taguchi method[17]. As shown in Table 3, A, B, C, and D respectively represent the four control factors of fin height, fin thickness, fin length, and fin spacing. Level 1, level 2, level 3, level 4, and level 5 respectively represent the five values under this structural parameter.

Table 3 Control factors and levels

Control factors	Level 1 (mm)	Level 2 (mm)	Level 3 (mm)	Level 4 (mm)	Level 5 (mm)
A	90	95	100	105	110
B	3	4	5	6	7
C	400	450	500	550	600
D	13	14	15	16	17

The key step of the Taguchi method is the establishment of the orthogonal table. After the selection of control factors and levels is completed, numerical simulation needs to be carried out in accordance with the principles of orthogonal experiments. The orthogonal table L25(5^4) is used for numerical simulation, as shown in Table 4.

Table 4 Numerical simulation scheme of the heat dissipation performance L25(5^4) of the heat sink

No.	A (mm)	B (mm)	C (mm)	D (mm)	SNR-*E* (dB)
1	90	3	400	13	-55.22
2	90	4	500	16	-55.47
3	90	5	600	14	-55.66
4	90	6	450	17	-54.42
5	90	7	550	15	-54.82
6	95	3	600	16	-56.59
7	95	4	450	14	-55.07
8	95	5	550	17	-55.37
9	95	6	400	15	-54.00
10	95	7	500	13	-54.48
11	100	3	550	14	-56.25
12	100	4	400	17	-54.75
13	100	5	500	15	-55.03
14	100	6	600	13	-55.27
15	100	7	450	16	-54.13
16	105	3	500	17	-55.94
17	105	4	600	15	-55.98
18	105	5	450	13	-54.64
19	105	6	550	16	-54.96
20	105	7	400	14	-53.77
21	110	3	450	15	-55.55
22	110	4	550	13	-55.67
23	110	5	400	16	-54.30
24	110	6	500	14	-54.63
25	110	7	600	17	-54.99

All 25 schemes are given a heat flux density of 30000 W/m^2 for the surface heat source and a fin movement speed of 50 m/s. The paper converts the comprehensive performance coefficient *E* into a logarithm-based Signal Noise Ratio (SNR) and processes the comprehensive performance coefficient *E* using the maximum characteristic formula. The formula is as follows:

$$\mathrm{SNR_L} = -10\lg\left(\frac{1}{n}\sum\nolimits_i^n \frac{1}{Y_i^2}\right) \tag{38}$$

The larger the data value of the large characteristic target value, the better its performance. The SNR values corresponding to the comprehensive performance coefficient *E* under 25 different structural parameter combinations are shown in Table 4.

Based on the SNR-*E* given in Table 4, the average SNR values of each control factor at each level were calculated. By calculating the range values of the average SNR of each control factor at different levels, the

influence of each control factor on the comprehensive performance coefficient E can be reflected. The larger the range value, the greater the influence of this control factor on the comprehensive performance of the heat sink. The calculation formula of the range R_m is as follows:

$$R_m = \mathrm{SNR}_{\max,i} - \mathrm{SNR}_{\min,i} \tag{39}$$

Table 5 shows the average SNR value and the range values under each control factor. Meanwhile, the range values are sorted to represent the influence of this control factor on the SNR value. The order of the influence of different control factors on the comprehensive performance coefficient E is as follows: fin thickness, fin length, fin height,and fin spacing.

Table 5 The influence effect of different control factors on the SNR value

—	Level	A (dB)	B (dB)	C (dB)	D (dB)
Average SNR-E	1	-55.12	-55.91	-54.41	-55.06
	2	-55.11	-55.39	-54.76	-55.08
	3	-55.09	-55.00	-55.11	-55.08
	4	-55.06	-54.66	-55.41	-55.09
	5	-55.03	-54.44	-55.70	-55.09
R_m	—	0.09	1.47	1.29	0.04
Ranking	—	3	1	2	4

The range can reflect the degree of influence of control factors on flow and heat dissipation, that is, the contribution rate of control factors to the comprehensive performance coefficient. Fig. 18 shows the contribution rate of each control factor to the comprehensive performance coefficient E.

$$\mathrm{Contribution}(i) = \frac{\mathrm{SNR}_{\max,i} - \mathrm{SNR}_{\min,i}}{\sum_{i=1}^{k}\left(\mathrm{SNR}_{\max,i} - \mathrm{SNR}_{\min,i}\right)} \tag{40}$$

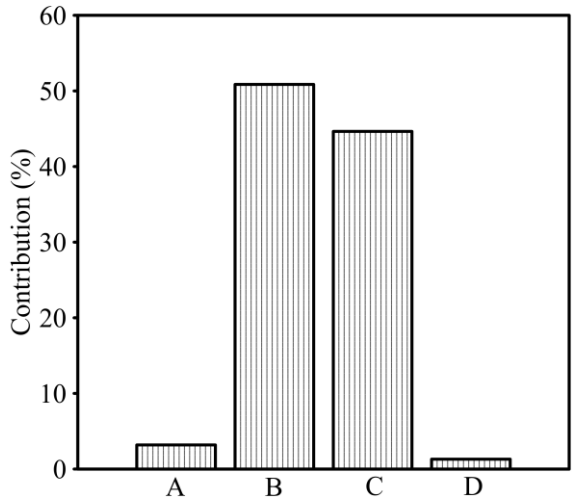

Figure.18 The contribution rate of each control factor to the comprehensive performance coefficient

V. CONCLUSION

The paper studies the convective heat transfer characteristics of the array fins on the outer surface of a moving object through numerical simulation methods. It mainly includes the air flow characteristics of the fin channel, the changes of surface convective heat transfer coefficient, heat transfer thermal resistance, fin efficiency, heat transfer coefficient, resistance coefficient, heat transfer factor and comprehensive performance coefficientunder different moving speeds. At the same time, the influence of fin structure parameters on the comprehensive performance of the heat sink was studied. The results show that:

(1) With the increase of the moving speed of the fins, the convective heat transfer coefficient on the surface of the fin channel increases, and the convective heat transfer capacity is enhanced.The paper uses the integration method to calculate the average temperature difference, and the heat transfer coefficient increases

with the increase of the train's moving speed.

(2) The thermal resistance of the fins decreases as the moving speed increases. The proportion of the heat conduction thermal resistance in the total thermal resistance becomes larger and larger. The decreasing speed of the heat conduction thermal resistance is slower than that of the convective thermal resistance, and the moving speed has a greater influence on the convective thermal resistance.

(3) The paper uses the integration method to calculate the average temperature difference in the heat transfer process, and the heat transfer coefficient increases with the increase of the movement speed of the fins.

(4) The comprehensive performance coefficient of the fins decreases as the moving speed of the fins increases, and the fin efficiency of also gradually decreases. This indicates that as the moving speed of the fins increases, the comprehensive performance of the fins will decline.

(5) The order of the influence of different structural parameters on the comprehensive performance of the heat sink is as follows: fin thickness, fin length, fin height,and fin spacing.

ACKNOWLEDGMENT

This work is supported by the National Nature Science Foundation of China (No. 52476076)

REFERENCES

[1] J.Y. Hu, C.D. Liu, F. Ye. A review on high-performance SiCf/SiC composites prepared by PIP process. *Journal of Materials Research and Technology*, 2024, 33: 7216-7235.
[2] K. Kobayashi, H.M. Peng.The main circuit system of Shinkansen vehicles is miniaturized and lightweight by using silicon carbide components.*Foreign Railway Locomotive and Motor Car*,2016,(04):32-36.
[3] X.B Pang, L.J. Kong, S. Wang. Application of train-induced wind cooling technology in traction equipment of rail vehicles [J]. *Railway Locomotive and Motor Car*, 2024, (11): 16-19.
[4] J. Jin. Research and application of natural air-cooled traction transformers for EMU. *Electric Drive for Locomotives*, 2024, (05): 1-11.
[5] J. Ma, M. Yang, B. Qian. Enhanced heat transfer for subway linear motor through underbody flow regulation. *International Journal of Heat and Mass Transfer*, 2024, 228: 125656.
[6] Q. Luo, H. Li, K. He. Research on the variation of wind speed around the traction converter of intercity EMU with vehicle speed. *Transport Business China*, 2023, (03): 1-3.
[7] N. Huang, Z.Y. Wu, X. Wang. Design of Running Air-cooling System for Subway Based on SiC Module. *Electric Drive for Locomotives*, 2020, (05): 62-66.
[8] Z. Lan, H.Y. Feng, W.Y. Liu. Study of rectangular fin heat sink performance and prediction based on artificial neural network. *Case Studies in Thermal Engineering*, 2024, 64: 105569.
[9] T. Saravanakumar, D.S. Kumar. Heat transfer study on different surface textured pin fin heat sink. *International Communications in Heat and Mass Transfer*, 2020, 119: 104902-104902.
[10] H. Dong, Q. Zhang, X. Yang. Sensitivity analysis and reasonable matching of key operating parameters of flow and heat transfer in liquid-cooling plate used for IGBT module of high-speed train traction inverters. *Case Studies in Thermal Engineering*, 2024, 61: 105056.
[11] I. Fuad, A. Ali, P. Yoav. Systematic micro heat sink optimization based on hydrofoil shape pin fins. *Case Studies in Thermal Engineering*,2021, (prepublish): 101028.
[12] H. Nemati, M.A. Moghimi, J.P.Meyer. Shape optimization of wavy mini-channel heat sink. *International Communications in Heat and Mass Transfer*, 2021, 122: 105172.
[13] O. Kosdere, Z. Sert, O. Altun. Investigation of thermal performance at forced convection in plate-fin heat sink. *Energy*, 2024, 307: 132621.
[14] W.Q. Tao. *Heat Transfer*. Beijing: Higher Education Press, 2019.
[15] J. Yun, K. Lee. Influence of design parameters on the heat transfer and flow friction characteristics of the heat exchanger with slit fins. *International Journal of Heat and Mass Transfer*, 2000, 43(14): 2529-2539.
[16] X.W. Xu, H. Li, Y. Bai. Numerical Simulation of Missile Vertical Thermal Launch Based onMoving Grid Layering Method. *Ship Electronic Engineering*, 2022, (09): 98-101.
[17] M. Tony. Book review: Taguchi methods - benefits, impacts, mathematics, statistics and applications. *Proceedings of the Institution of Mechanical Engineers*, Part B: Journal of Engineering Manufacture, 2012, 226(11): 112-120